Energy deposition at the probe surface under plasma conditions typical for ion thruster

IEPC-2011-270

Presented at the 32nd International Electric Propulsion Conference,
Wiesbaden • Germany
September 11 – 15, 2011

A.Cenian[1], A.Chernukho[2], H.Rachubiński[3],
The Szewalski Institute of Fluid-Flow Machinery, PASci, 80-952 Gdańsk, ul. Fiszera 14, Poland

and

M.Dudeck[4]
University of Paris 6, 75252 Paris, France

Abstract: In this work an energy deposition at the probe surface immersed in the Xe plasma of the ion thruster is investigated. The extensive investigations were performed using the PIC MC code in order to check the effect of various secondary electron emission (SEE) processes on power deposited at the surface.

Nomenclature

E_n = radial field value at the n-th grid point
S_n = $2\pi r_n l$ is the surface of the n-th grid element of radius r_n
Q_{+n} (Q_{-n}) = the ion (electron) charge accumulated in the n-th grid element
$n_e(x)$ = electron profile
T_e = electron temperature
T_i = ion temperature
r_b = $(3/2)^{1/2} r_s$ plasma bulk zone
r_s = the radius of the SPS zone
$\gamma(w,\upsilon)$ = the total SEE coefficient as a function of electron impact energies w and impact angles υ
$\gamma_t(w,\upsilon)$, $\gamma_e(w,\upsilon)$, $\gamma_i(w,\upsilon)$ = the coefficient of true, elestic and inelstic contribution to $\gamma(w,\upsilon)$

I. Introduction

THE Langmuir probe is a well-established diagnostic tool for a low pressure, stationary plasma. Most of the analytical probe theories were developed under the assumption of a collisionless probe-sheath (ion motion determined by electric field), a Boltzmann electron profile ($n_e(x) = n_{e0} \exp[-eU(x)/kT_e]$) and a constant electron to ion temperature ratio, T_e/T_i (see e.g. ref. 1).

Parallel to various analytical models, some numerical models based on the PIC-MC method have recently been developed for a Langmuir probe[2,3,4] and ion thruster[5].

Kawamura and Ingold[6] have proposed a 1d3v (1D in space displacement, 3D in velocity) PIC-MC model of an electropositive plasma for cylindrical-symmetry systems. The 3D trajectories are calculated in this model but only the radial (1D) charge distribution is taken into account in Poisson's equation (taking advantage of the assumed symmetry). Both elastic and inelastic (excitation and ionisation) collisions of electrons with Ar atoms were considered. Only elastic processes (isotropic and backscattering) were taken into account for the calculation of ion trajectories. Preliminary investigations[7] have already proved that this type of model could be useful to study some fundamental problems of plasma-wall interactions, including plasma neutrality, the Bohm criterion and the sheath formation. The above mentioned models[2,6] served as a background for modelling of cylindrical probes immersed in

[1] Prof. of IFFM, Department of Physical Aspects of EcoEnergy, cenian@imp.gda.pl
[2] Specialist, Department of Physical Aspects of EcoEnergy, chernukh@itmo.by
[3] PhD student, Department of Physical Aspects of EcoEnergy, hrachubinski@imp.gda.pl
[4] Prof., Institut d'Alembert, dudeck@lmm.jussieu.fr

high and low pressure plasma[3,4]. The first current-voltage, I-V, characteristics of the probes determined using PIC MC method were discussed there.

In the presented paper, the PIC-MC model, developed by Cenian et al.[4] for an electrical probe in an Ar plasma[8], is extended in order to include the process of Secondary Electron Emission (SEE) – see e.g. Ref. 5. Also, all the necessary data to enable consideration of Xe plasma under conditions close to those observed in ion thrusters are included.

II. Model of plasma-surface interactions

A. Geometry and general description of the model

The plasma-probe interactions are studied in a system with cylindrical symmetry, related to an infinitely long cylindrical probe, $2r_p$ in diameter, immersed in a continuum, electro-positive plasma. For the sake of simplification, the whole plasma volume is separated into two different zones: Sheath-Pre-Sheath (SPS) zone and a ring-shaped volume around it (referred to hereafter as plasma bulk zone) – see Fig. 1. The considered radius of the SPS zone depends strongly on the probe bias voltage as was discussed in Ref. 4. The motion of charged particles in both zones is described by the MC trajectories.

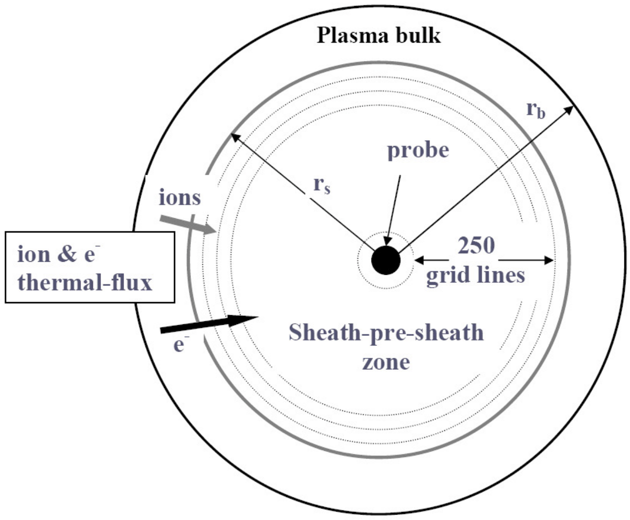

Figure 1. Scheme of the considered zones in the PIC-MC model; 250 radial grid lines are presented by dotted circles.

The concentration of charged particles in the plasma bulk zone is kept constant by assuming that the particles reflect specularly at the boundaries i.e. at the boundary with the SPS zone and at an external boundary given by r_b (radius of plasma bulk zone). The neutral plasma of the plasma bulk is described by the electron (T_e) and ion (T_i) “effective” temperatures (see ref. 9). Maxwell distributions were generally assumed as the initial conditions, but other distributions may be easily introduced as well. As the simulations continue, the charged particle distribution changes drastically. Initially, the charged particles are uniformly distributed in the whole considered space, i.e. plasma bulk and SPS zones. Later, the charged particle densities begin to decay in the close vicinity of the probe, due to the constant flux towards the probe and absorption (followed by recombination) or secondary electron emission (see next chapter) on the probe surface. On the other hand, there is a continuous thermal influx of charged particles from the plasma bulk zone to the SPS zone. This flux is simulated by the creation of a particle entering the SPS zone, with the same velocity as the particle from the plasma bulk zone which was reflected from the border with the SPS zone. When a particle is crossing the same boundary but from the SPS side, it is removed from the simulation.

Hence, the charged particles are specularly reflected at the $r = r_b$ boundary in the bulk plasma zone. Whenever a particle from the bulk plasma zone approaches the $r = r_s$ boundary it is specularly reflected back to the zone but the twin-particle continues also its movement in the SPS zone i.e. an additional particle is generated in that zone. The particles are neglected when approaching the $r = r_s$ boundary from the SPS side. The described procedure makes it possible to keep the charged particle density (ionization degree) in the plasma bulk zone constant, and it also enables us to determine the thermal flux from the plasma bulk to the SPS zone. It was verified that though the described procedure is simpler it gives the same results as the one used previously[3]. It should be noted here that the flux from the plasma bulk into the SPS zone is higher than that in the opposite direction, giving a net thermal influx of charged particles to the SPS zone.

The charged-particle MC trajectories in the SPS zone are determined by the Newtonian equations for particles motion in electric and magnetic fields. It is possible to take into account both the axial-field of the DC plasma column (if such exist) as well as the radial field generated by the probe-bias and the space-charge density (through the Poisson equation evaluated in 250 grid points) – see Fig. 1. The potential is derived from the integral form of Poisson equation

$$E_i \bullet S_i = 4 \pi \Sigma_{n=1,i} \; [Q_{+n} - Q_{-n}] \,,$$

where E_n is the radial field value at the n-th grid point, $S_n = 2\pi r_n l$ is the surface of the n-th grid element of radius r_n and Q_{+n} (Q_{-n}) is the ion (electron) charge accumulated in the n-th grid element. It should be noted that the surface S_n the charges Q_{+n} and Q_{-n} as well as other extensive quantities are calculated per unit length in the model.

The outer radius of the plasma bulk zone, r_b , is related to the radius of the SPS zone, r_s , by the relation $r_b = (3/2)^{1/2} r_s$, which ensures that initially in the plasma bulk zone the number of charged particles is ~ 50% of the number of charged particles in the SPS zone. This can be explained by taking into account the initially uniform spatial distribution of charged particles and by neglecting the volume filled by the probe. Initially, the trajectories of 6000 - 9000 super-particles in the SPS zone were calculated. Later, this number fluctuates, as some particles are being lost on the SPS borders and others are created, when the charge particles enter the SPS zone as described above. It was found that, the ionisation processes play only a marginal role in the creation of charged particles in this zone.

The electrons on their way to the probe take part in different collision processes with the Xe atoms. Cross section for the elastic collisions are from Hayashi[10], for the excitation processes from Sydorenko[5] and for the step ionization from Phelps[11]. The electron-electron collision processes are ignored.

B. Processes at the surface

The probe surface was assumed to be fully absorptive both for electrons and ions in Ref 4, i.e. a particle was removed from the simulation (absorbed on the probe surface and recombined) when its trajectory passes the probe-wall coordinate (i.e. when $r < r_p$). The difference between the number of absorbed electrons and ions determines the probe current. Here, we include also other processes at the probe surface, i.e. the possibility of electron reflection from the probe surface and emission of secondary electrons. The processes are described based on the procedure developed by Vaughan[12] and later modified by Sidorenko[5]. So, here electrons can: (i) be absorbed, (ii) be reflected specularly or at a random direction, either elastically or inelastically, (iii) cause the emission of secondary electrons – see Fig. 2. The description doesn't include SSE emission due to the UV-wall interaction.

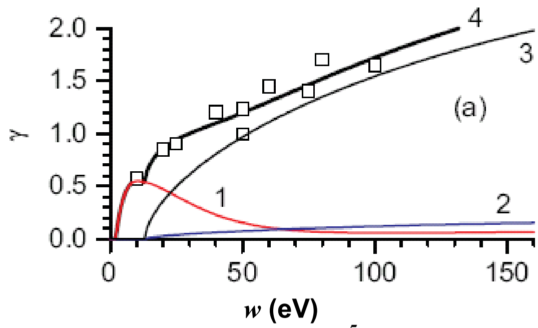

Figure 2. (after Siderenko[5]): The emission coefficients of the components of secondary electron emission versus the incident electron energy for normal incidence (υ=0); curve 1 is the elastic reflection γ_e; curve 2 the inelastic backscattering γ_i; curve 3 the true secondary emission γ_t; and curve 4 the total emission coefficient γ. Squares mark the available experimental data for boron nitride ceramics used in ion thrusters.

The general phenomenological model of SEE[12,13] assumes that the total flux of secondary electrons F_2 consists of (i) elastically reflected primary electrons with flux F_{2e} , (ii) inelastically backscattered primary electrons with flux F_{2i} , and (iii) true secondary electrons with flux F_{2t} , i.e., $F_2 = F_{2e} + F_{2i} + F_{2t}$. The emission coefficients for these processes are defined by the relationship $\gamma_{e,i,t} = F_{2e,i,t}/F_1$, where F_1 is the total primary electron flux.

The total SEE coefficient

$$\gamma(w,\upsilon) = F_2(w,\upsilon)/F_1(w,\upsilon) = \gamma_t(w,\upsilon) + \gamma_e(w,\upsilon) + \gamma_i(w,\upsilon) \tag{1}$$

as a function of electron impact energies w and impact angles υ is well described by the Vaughan's coefficient $\gamma_V(w,\upsilon)$ – see Ref.12 or 5, for higher values of w, but it differs from γ_V rather substantially for lower w values.

As shown in Fig. 2, at low impact energy the **elastic reflection** is the most probable process (γ_e reaches value ~0.5 at primary electron energy w = 5–10eV [9]); at high energies the flux of elastically reflected electrons constitutes only about 3% of total flux. The function $\gamma_e(w,\upsilon)$ for the incident impact angle $\upsilon=0$ is presented in Fig. 2 by curve 1. The energy of elastically reflected electrons is equal to the energy of incident electrons.

The current due to the **inelastically backscattered electrons** is about 7% of the total secondary flux F_2 [14] – see curve 2 in Fig. 2. The energies of inelastically backscattered electrons are assumed to be uniformly distributed between 0 and incident electron energy w.

The **true secondary emission coefficient** is set to [5]

$$\gamma_t(w,\upsilon) = (1 - r_e - r_i)\,\gamma_V(w,\upsilon)\ . \tag{2}$$

where re = 0.03 and r_i = 0.07 – see curve 3 in Fig. 2. The energies of true secondary electrons are emitted with energies corresponding to a half-Maxwellian distribution of temperature T_t

$$f_t(w) = \frac{2w^{1/2}}{\pi^{1/2}T_t^{3/2}} \exp\left(-\frac{w}{T_t}\right) . \tag{3}$$

III. Results

The Langmuir probe characteristic has been investigated under conditions related to Xe plasma in ion thruster, i.e. N =[Xe] = 1.6 ×10^{13} cm^{-3}, n_e = 1.2×10^{12} cm^{-3}, T_e = 14 eV. The probe considered had diameter D_{probe}= 2 r_p = 626 µm and the width of the sheath equal 30 λ_D was assumed. The VAC characteristic of Langmuir probe in Ar and Xe plasma under similar conditions has been compared in Fig. 3. The differences only marginally exceed 10%.

Figure 4 presents the role of various emission processes: elastic, inelastic and true secondary emissions. The four different combinations of coefficients are considered:

1. $\gamma = 0$
2. $\gamma_e = 0.5,\ \gamma_i = 0,\ \gamma_t = 0;$
3. $\gamma_i = 0.5,\ \gamma_e = 0,\ \gamma_t = 0;$
4. $\gamma_t = 0.5,\ \gamma_i = 0,\ \gamma_e = 0.$

Surprisingly, only the elastic processes – case (2) – lead to substantial difference in relation to case (1), describing the case without any secondary emission. The curves 1 and 4 practically coincide i.e. the true secondary emission processes do not influence the IV probe characteristic. This is related to the fact that the secondary electrons are slowed down (if compared to primary ones) and take part in absorption and recombination on the probe (in the case of positive voltage).

The effect of secondary electron emission and magnetic field on floating potential has also been studied – see Figs. 5 and 6. It has been shown that as the SEE coefficient grows a floating potential gets less negative values. Besides, Fig.5. shows that elastic collisions produce more significant effects than true SEE. It can be seen that increase of SEE coefficient from zero to 0.5 can change the value of floating potential by about 15 V.

The influence of axial field on probe characteristic is stronger because axial field deflect all electrons approaching the probe from any direction in plane perpendicular to the probe axis (direction of electric field).

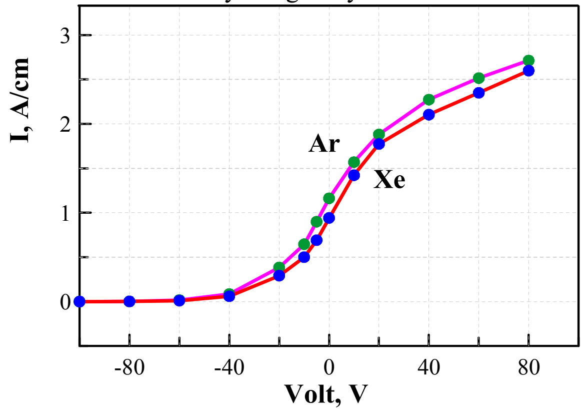

Figure 3. Comparison of calculated VAC in Ar and Xe plasma

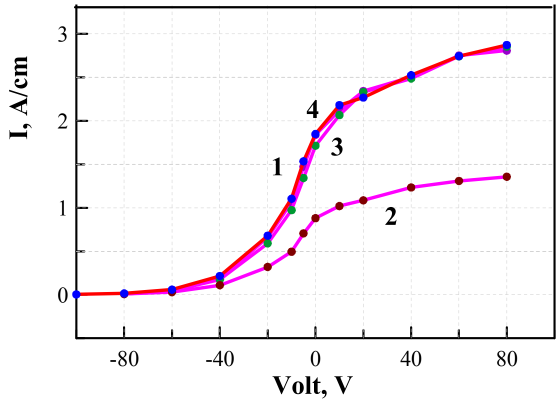

Figure 4. Comparison of calculated VAC with different secondary electron emission coefficients

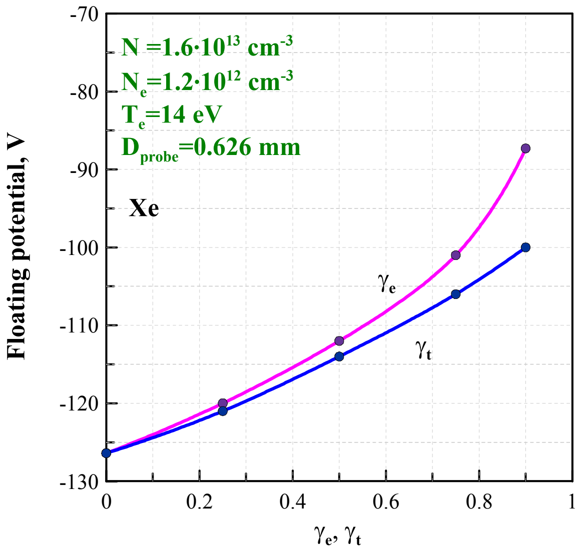

Figure 5. Effect of secondary electron emission on floating potential

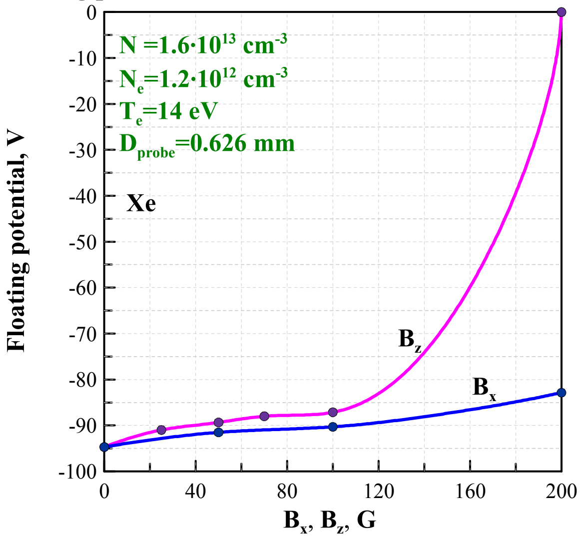

Figure 6. Dependence of floating potential on axial and radial magnetic field

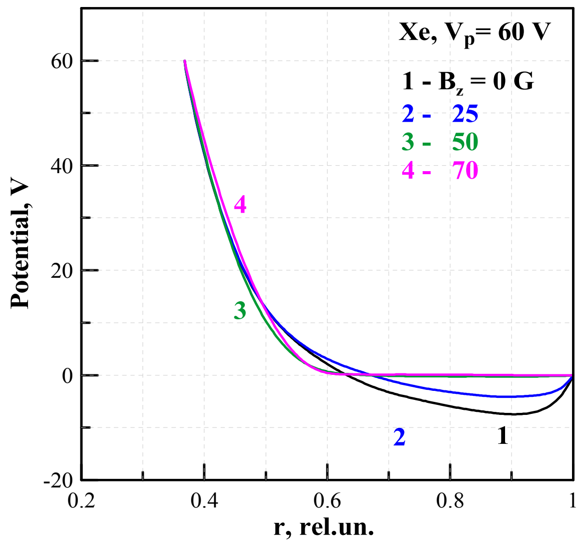

Figure 7. Potential profile for different axial magnetic fields

For radial B-field the electrons moving radially are not influenced at all.

Figure 6 shows the dependence of floating potential on axial (B_z) and radial (B_x) magnetic field. In the case of the axial field the floating potential decreases (in relation to the case without field) even by about 95 V, when the field reaches value of about 200 G.

Besides, the potential at the vicinity of probe surface was determined and its dependence on axial magnetic field was discussed – see Fig. 7. The potential well is flattened as the magnetic field increases.

In this work an energy deposition at the probe surface immersed in the Xe plasma of the ion thruster under conditions described in Ref. 15 and the effect of various secondary electron emission (SEE) is investigated. Figure 8 presents the power deposited per probe length of 1 cm, with various (elastic, true and total) and without SEE processes. One sees that SEE processes lead to decrease of energy deposition. The elastic processes are more efficient in the power reduction.

The axial magnetic field also leads to substantial power reduction – see Fig. 9. Electrons deflected on their route to the probe collide with its surface significantly less frequently. This research will be extended for an analysis of the plasma energy deposition on the insulated walls of the channel of Hall thrusters.

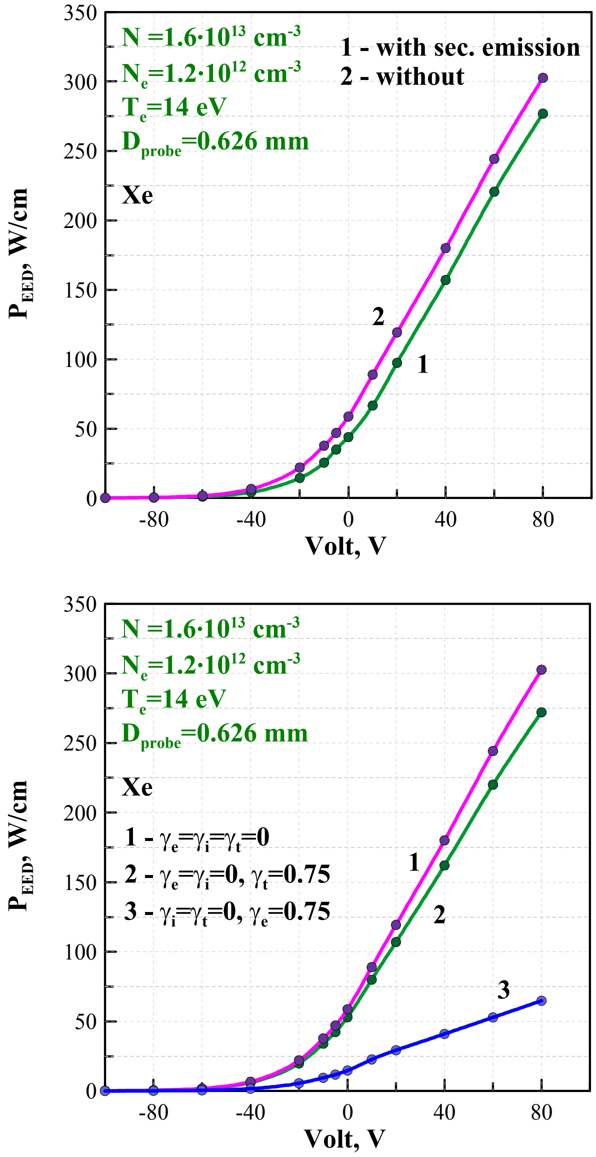

Figure 8. Electron energy deposition on probe surface (a) with (for surface covered by boron nitride ceramics) and without secondary electron emission; (b) for elastic and true SEE processes

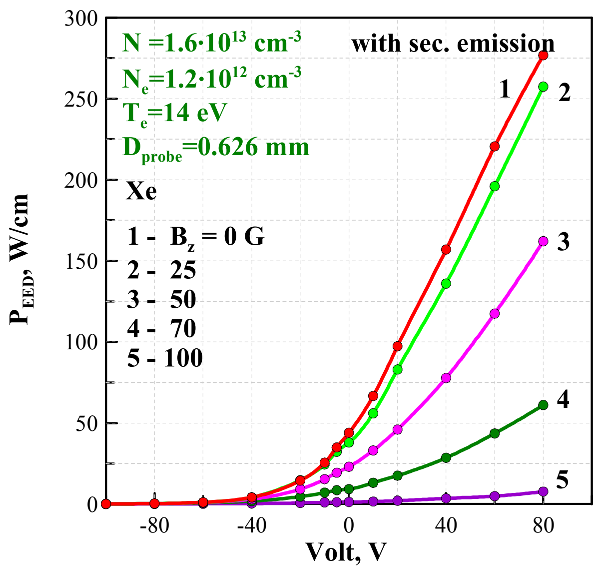

Figure 9. Influence of axial magnetic field on electron energy deposition on probe surface.

IV. Conclusions

It was shown that the discussed PIC MC model described in Ref. 4 and verified using measured IV characteristics of Langmuir probe immersed in the well described plasma can be applied to study plasma under conditions close to that in ion thrusters. The secondary electron emission influences the IV characteristic of Langmuir probe especially at positive voltages. However, only elastic reflection processes really contribute significantly to the probe current.

The elastic SEE processes reflect electrons from probe with the same relatively high speed. This leads to a more or less uniform increase of electron density in the sheath. It does not influence electron density close to of probe surface.

It was observed that the axial magnetic field influences probe characteristics and floating potential more significantly than radial field. The axial field deflects all electrons approaching probe.

Acknowledgments

This research has been performed during realization of the project n°3161 “Propulsion par plasma dans l’espace” financed by the Groupement De Recherche CNRS/CNES/Snecma/Universités.

References

[1]Mott, H. and Langmuir I., " The theory of collectors in gaseouns discharges," *Phys.Rev.*, Vol. **28**, No. 4, 1926, pp.727-763.

[2] Kono A., "Complex sheath formation around a spherical electrode in electronegative plasmas: a comparison between a fluid model and a particle simulation," *J.Phys.D: Appl.Phys.*, Vol. **34,** No. 7, 2001, pp.1083-1090

[3]Cenian A., Chernukho A., Bogaerts A. and Leys C., "Plasma-surface interactions for langmuir probe immersed in hydrocarbon combustion front," *Khim. Fiz.,* Vol. **23,** No.9, 2004, pp. 3-7.

[4]Cenian A., Chernukho A., Bogaerts A., Gijbels R. and Leys C., "Particle-In-Cell Monte Carlo (PIC-MC) modelling of Langmuir probes in an Ar plasma," *J.Appl.Phys.,* Vol. **97**, No. 12, 2005, pp. 123 310-123 320.

[5]Sydorenko D.: "Particle-in-Cell Simulations of Electron Dynamics in Low Pressure Discharges with Magnetic Fields," Ph.D. Dissertation, Department of Physics and Engineering Physics, University of Saskatchewan, Saskatoon, 2006.

[6]Kawamura E. and Ingold J.H., "Particle in cell simulations of low pressure small radius positive column discharges," *J.Phys.D: Appl. Phys.*, Vol. **34,** No. 21, 2001, pp. 3150-3163.

[7]Cenian A., Chernukho A. and Leys C., "Particle-in-cell Monte Carlo (PIC-MC) simulations of plasma–wall interactions in low-pressure AR plasma," *Radiation Phys. and Chem.* Vol. **68,** No.1-2, 2003, pp.109-113

[8]Sternovsky Z., Robertson S. and Lampe M., "Ion collection by cylindrical probes in weakly collisional plasmas: Theory and experiment," *J.Appl.Phys.*, Vol.**94,** No.3, 2003, pp.1374-1381.

[9]Godyak V. A., Piejak R. B. and Alexandrovich B. M., "Probe diagnostics of non-Maxwellian plasmas," *J.Appl.Phys.*, Vol. **73**, No. 8, 1993, pp.3657-3663.

[10]Hayashi M., "Calculation of swarm parameters in xenon at high E/N by a Monte Carlo simulation method," *J.Phys.D: Appl. Phys.* Vol.16, No. 4, 1983, pp.581-590.

[11]Phelps A.V., "Compilation of electron cross sections used at JILA," [online database], URL:ftp://jila.colorado.edu /collision_data/electronneutral/electron.txt [cited 15 October 1997].

[12]Vaughan J. R. M.. "A new formula for secondary emission yield," *IEEE Trans. Electron Devices*, Vol. **36**, No. 9, 1989, pp. 1963-1967, 1989.

[13]Seiler H., "Secondary electron emission in the scanning electron microscope," *J. Appl. Phys.*, Vol. **54**, No. 11, 1983, pp. R1-R18.

[14]Gopinath V. P., Verboncoeur J. P. and Birdsall C. K., "Multipactor electron discharge physics using an improved secondary emission model," *Phys. Plasmas*, Vol.**5**, No. 5, 1998, pp.1535-1540.

[15]Boeuf J. P. and Garrigues L., "Low frequency oscillations in a stationary plasma thruster," *J. Appl. Phys.*, Vol. **84**, No. 7, 1998, pp.3541 - 3554